# Nonlinear Response to Picosecond Pulse Excitations in Magneto-Dielectric Media

Hoton How, C. Vittoria, *Fellow, IEEE,* and K. Trott

***Abstract*—Nonlinear responses of magneto-dielectric thin layers to picosecond excitation have been calculated utilizing direct time-domain integration. Relaxations, hysteresis, and magnetic saturation phenomena associated with the response are therefore discussed in depth. The purpose of this calculation was to provide an analytical method by which physical properties of materials can be identified under picosecond-pulse excitation as well as to explore special cases of excitations in which picosecond pulses are efficiently absorbed. The calculations indicate that by examining the reflected waveform of the incident rectangular picosecond pulse the amount of magnetic hysteresis and saturation of the material may be estimated. It is shown that magnetic hysteresis will affect the shape of the trailing edge of the reflected signal, whereas the magnetic saturation effect can be identified from the slope of the reflected pulse step. Examples of designing effective picosecond-pulse screening structures have also been illustrated.**

## I. Introduction

FOR YEARS there has been great interest in the radar and survivability communities concerning the response of materials to narrow picosecond pulse excitation. There are two basic methods for calculating the response. One approach is to assume that the fields in Maxwell equations are macroscopic fields. Relaxation effects are introduced phenomenologically. The system is assumed to be in thermodynamic equilibrium even during the period of relaxation time for the system. Nonlinear effects are coupled into Maxwell equations of motion via the medium polarization vectors. The other approach is to introduce relaxation and nonlinear effects at the microscopic level of computation using Fermi's equation for transition rates, for example. Macroscopic fields may be calculated by averaging over the possible quantum states and proper probability distribution function from the so-called master equation at a given temperature [1]. For pulse widths of 1 picoseconds or greater the former approach is reasonable in view of atomic transition rates being much faster than relaxations. We used this approach in an earlier paper to analyze nonlinear effects in magnetic media even in the presence of small amplitude pulsed fields [2]. This is due to the B-H hysteresis curve associated with irreversible processes as in domain wall motions. We approximated the time response by assuming two different magnetic permeabilities for the partial waves associated with the rising and the falling edges of the applied picosecond pulse [2]. Therefore, the permeability value was assumed to change coherently in time throughout the material. Actually, due to internal reflection and relaxation effects the material responds to the applied excitation pulse quite incoherently for different parts of the material. This requires a detailed record of the magnetization history at every point of the material.

We have now calculated the response in the time domain and the results have been compared to those associated with frequency-domain calculations. Previous frequency-domain calculations predict quite accurately the front and trailing edges of the reflected signal. However, the tail to the reflected signal is slightly greater than that predicted by the exact time-domain calculations.

Section II formulates the iteration scheme for a time-domain integration. The material considered possesses both relaxation times in the electric and magnetization polarization vectors. The magnetization is assumed saturatable and hysteretic. Calculated results given in Section III illustrate the difference in picosecond responses for different material parameters. A novel trapping/absorption process is suggested in Section III which may be important for the design of microwave absorption for incident picosecond pulses. Discussions and conclusions are summarized in Section IV.

## II. Calculations

Fig. 1 shows a metal-backed magneto-dielectric slab of thickness a. Consider a rectangular pulse of duration $\Delta t$, which is applied at time $t = 0$. The pulse is traveling along the $z$-axis, which is normal to the front surface of the metal-backed slab. The magnetization process is shown in Fig. 2. Initially, the magnetization is zero in the absence of an external magnetic field. An unmagnetized magnetic state can be realized if the medium consists of multi-domains. The magnetic domains are randomly oriented so that the net magnetization along any direction is zero. The hysteresis loop associated with this type of magnetic state is typically shown in Fig. 2. Since we have assumed magnetic domains in the medium, there exist minor and so-called major hysteresis loops. The size of the loops is directly related to the amplitude of the driving field of the pulse amplitude. We have simplified the shape of the hysteresis loop in order to demonstrate the calculational method. Furthermore, no precessional motion of the magnetic domain is assumed upon the application of the pulse field.

Fig. 2 depicts the magnetization processes as follows. As $H$ is increased above 0, $M$ defines a line along $OA$. However, if $H$ decreases in amplitude at point $A, M$ will decrease

Manuscript received February 19, 1992; revised May 18, 1992. This work was supported by the Air Force Office of Scientific Research, and the Target Characterization of Rome Laboratory at Hanscom AFB MA

H. How and C. Vittoria are with the Electrical and Computer Engineering Department, Northeastern University, Boston, MA 02115.

K. Trott is with Rome Laboratory, RL/ERCT, Hanscom AFB, MA 01731.

IEEE Log Number 01731.

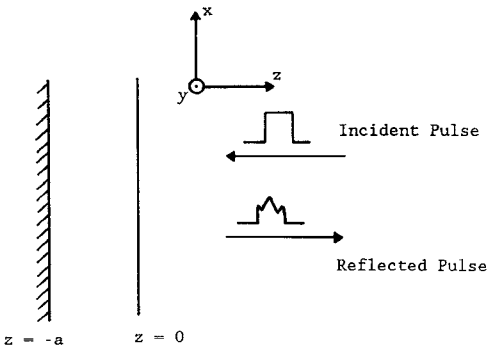


Fig. 1. Pulse incidence on a metal backed slab.

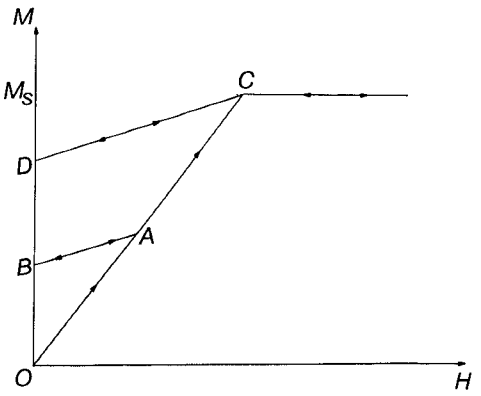


Fig. 2. Nonlinear magnetization processes.

accordingly along the line $AB$. In some sense a minor loop is traced out as the pulse field is applied. Increasing $H$ afterward will magnetize the material along line $BA$ until point $A$ is reached after which magnetization takes place along line $AC$. Further increase of $H$ will retain $M$ at $M_s$, since $M$ is assumed to be saturated at $M_s$. A decrease of $H$ will lead $M$ to decrease along Line $CD$. Lines $AB$ and $CD$ trace out a minor loop of a magnetic hysteretic material. We assume lines $AB$ and $CD$ are of slope $\chi_m^{(-)}$, which is different from $\chi_m^{(+)}$, the slope of line $OC$. We note that Fig. 2 shows the magnetization response only for quasi-static processes. For rapid magnetization changes under slow magnetic relaxations, $M$ lags $H$ significantly and the horizontal axis of Fig. 2 must be interpreted as the delayed $H$ field at previous time at the same spatial location, see (2c) below.

The governing equations are Maxwell equations (in MKS units)

$$\frac{\partial E}{\partial z} - \frac{\partial}{\partial t}(H + M) = 0, \tag{1a}$$

$$\frac{\partial H}{\partial t} - \frac{\partial}{\partial t}(E + P) = 0, \tag{1b}$$

where we consider only the one- dimensional case with $H, M$ and $E, P$ parallel to $x$, and $y$, respectively. The constituent equations for $M$ and $P$ are

$$\tau_e \frac{\partial P}{\partial t} + P = \chi_e E,$$

$$\tau_m \frac{\partial M}{\partial t} + M = \chi_m^* H + C^*, \text{if } M < M_s, \tag{2a}$$

or

$$M = M_s, \text{otherwise.} \tag{2b}$$

Here $\tau_e$ and $\tau_m$ denote dielectric and magnetic relaxation times, respectively, and $\chi_e$ and $\chi_m^*$ are dielectric and magnetic susceptibilities. $\chi_m^*$ can be either $\chi_m^{(+)}$ or $\chi_m^{(-)}$, depending on which magnetization curve that the magnetization process follows. In (2a) and (2b) $E$ and $H$ may represent instant electric and magnetic fields, but $C^*$ must be extrapolated through the magnetization process. For process along $OC$ $C^* = 0$, and

$$C^* = (\chi_m^{(+)} - \chi_m^{(-)}) M_A / \chi_m^{(+)} \tag{2c}$$

for process along $AB$, where $M_A$ denotes magnetization value of the process at point $A$. Due to time-delay in the process, the instantaneous $H$ field at point $A$ shouldn't be used in deriving $C^*$ in (2c). In the following $E$ and $H$, and hence, $P$ and $M$, are normalized with respect to the incident pulse amplitudes, and $z$ and $t$ are normalized to $c\Delta t$ and $\Delta t$, respectively. Here $c$ denotes the velocity of light in vacuum and $\Delta t$ is the duration of the incident picosecond pulse. Note that $M$ and $P$ can take only positive values under the present consideration. In air, $z > 0, M$ and $P$ vanish. The boundary conditions require $E$ and $H$ to be continuous across the air-layer interface at $z = 0$. At $z = -a$ perfect electric wall boundary conditions are imposed: $E = 0$ and $\partial H/\partial z = 0$.

Equations (1) and (2) can be integrated using the implicit second-order method. The Lax–Wendroff scheme is therefore employed in which numerical instabilities can be readily suppressed [3]. Denote $\delta t$ and $\delta z$ as the timestep and grid space, respectively. Let $E_j^n$ be the electric field at $z_j$ and $t_n$, etc. One may define intermediate field, say $E_{j+1/2}^{n+1/2}$, at the half timesteps $t_{n+1/2}$ and the half mesh points $z_{j+1/2}$. The calculational scheme is as follows

$$P_j^{n+1/2} = P_j^n + \frac{\delta t}{2}(\chi_e E_j^n - P_j^n)/\tau_e, \tag{3a}$$

$$M_j^{n+1/2} = M_j^n + \frac{\delta t}{2}(\chi_m^* H_j^n - M_j^n + C_j^*)/\tau_m, \tag{3b}$$

$$E_{j+1/2}^{n+1/2} = \frac{1}{2}\Big[E_{j+1}^n + E_j^n + P_{j+1}^n + P_j^n - P_{j+1}^{n+1/2} - P_j^{n+1/2} + \frac{\delta t}{\delta z}(H_{j+1}^n - H_j^n)\Big] \tag{3c}$$

$$H_{j+1/2}^{n+1/2} = \frac{1}{2}\Big[H_{j+1}^n + H_j^n + M_{j+1}^n + M_j^n - M_{j+1}^{n+1/2} - M_j^{n+1/2} + \frac{\delta t}{\delta z}(E_{j+1}^n - E_j^n)\Big] \tag{3d}$$

$$P_j^{n+1} = P_j^n + \delta t[\chi_e(E_{j+1/2}^{n+1/2} + E_{j-1/2}^{n+1/2})/2 - P_j^{n+1/2}]/\tau_e, \tag{4a}$$

$$M_j^{n+1} = M_j^n + \delta t[\chi_m^*(H_{j+1/2}^{n+1/2} + H_{j-1/2}^{n+1/2})/2 - M_j^{n+1/2} + c_j^*]/\tau_m, \tag{4b}$$

$$E_j^{n+1} = E_j^n + P_j^n - P_j^{n+1} + \frac{\delta t}{\delta z}(H_{j+1/2}^{n+1/2} - H_{j-1/2}^{n+1/2}), \tag{4c}$$

$$H_j^{n+1} = H_j^n + M_j^n - M_j^{n+1} + \frac{\delta t}{\delta z}(E_{j+1/2}^{n+1/2} - E_{j-1/2}^{n+1/2}). \quad (4d)$$

We note that (1a) and (1b) represent coupled partial differential equations of the hyperbolic type only if $\tau_e$ and $\tau_m$ in (2a) and (2b) are zero. In the presence of damping (1a) and (1b) are actually coupled parabolic partial differential equations which admits diffusion-like solutions. Damping dissipates energy and can be related to real physical processes such as electron-phonon scattering (electric conductivity) and magnon-phonon scattering (spin relaxation), etc. For partial differential equations of both types one must have $\delta t \leq \delta z$ such that conditions for von Neumann instabilities [3] are avoided as (1a) and (1b) are integrated in the time domain, (3a) to (4d). To avoid numerical dispersion $\delta t = \delta z$ should be used for the hyperbolic-type equations. For parabolic-type equations one must have the timestep smaller than the damping times so as not to introduce nonphysical solutions. Finally, mesh-drift instability can be avoided in the above integration scheme if one adds to the right sides of (4c) and (4d) small numerical damping terms (numerical viscosities) [4].

## III. Calculational Results

In the following calculations we adopt identical physical parameters used in [2]. For ferrites $4\pi\chi_m^{(+)}$ can be estimated approximately from $4\pi\chi_m/H_A$, where $4\pi M_s$ is the saturation magnetization and $H_A$ the magnetic anisotropy field. For spinel ferrites, for example, $4\pi M_s \approx 3000$ G and $H_A \approx 300$ Oe so that $4\pi\chi_m^{(+)}$ is about 10. $4\pi\chi_m^{(-)}$ is therefore smaller than 10, and $4\pi\chi_m^{(-)}$ equals 10 if there is no magnetic hysteresis. Under multidomain excitations at zero dc field the magnetic slab exhibit a linewidth $\Delta f$ roughly equal to $\gamma 2\pi M_s$, where $\gamma$ is the gyromagnetic ratio. Magnetic damping is directly related to this linewidth and the associated relaxation time is approximately $\tau_m \approx 1/\Delta f$. For $4\pi M_s$ is the order of kilogause $\tau_m$ turns out to be a few tenth of nanoseconds. Dielectric relaxation is usually much faster than magnetic relaxation times and dielectric relaxation time $\tau_e$ is in the order of picoseconds for normal oxide insulators. $\chi_\epsilon$ ranges from 5 to 15 for normal ferrite oxides.

Fig. 3 shows a comparison between the time-domain and the frequency-domain calculations [2]. In this figure the reflected $H$ field is plotted against normalized time assuming the following parameters: $\chi_e = 10, \chi_m^{(+)} = 10, \tau_e = 0.2, \tau_m = 2, a = 1/15$, and $M_s \gg 1$ (magnetic nonsaturable). Curve (1) is for the nonhysteretic case, $\chi_m^{(-)} = 10$, and curves (2) and (3) are for the hysteretic case, $\chi_m^{(-)} = 5$. Curve (1) was calculated using both time-domain and frequency-domain methods, curve (2) is the results for time-domain calculations, while curve (3) is that derived from frequency-domain calculations [2]. In the frequency-domain treatment 4000 Fourier terms have been incorporated in the calculations and ripples are still visible as revealed in Fig. 3. For the nonhysteretic case the two methods provide exactly the same results, indicating that the calculational scheme outlined in (3a) to (4d) is efficient in calculating the time-domain results. For

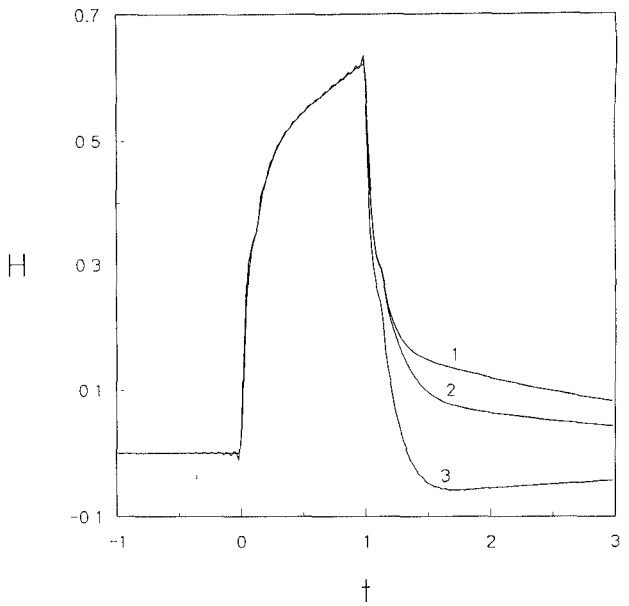


Fig. 3. Magnetic hysteretic effects calculated in the time and frequency domains: $\chi_e = 10, \chi_m^{(+)} = 10, \tau_e = 0.2, \tau_m = 2, a = 1/15, M_s \gg 1$. Curve (1): $\chi_m^{(-)} = 10$, time and frequency domains Curve (2): $\chi_m^{(-)} = 5$; time domain. Curve (3): $\chi_m^{(-)} = 5$; frequency domain.

the hysteretic case curves (2) and (3) coincide in the reflected waveforms concerning the rising edge and the following-up step. However, for times away from the edges the time-domain solution deviates from the frequency domain solution. The difference in the two solutions is due to the assumption for the frequency domain solution that the magnetic permeability is switched from $\chi_m^{(+)}$ to $\chi_m^{(-)}$ coherently in time all over the whole material and the partial waves of the two step edges can react separately with the material. Therefore, the frequency domain approach gives rise to approximate solutions at times greater than the duration of the incident pulse. However, the mathematical convenience of the frequency-domain approach is that the frequency response is easily obtainable without any Fourier transformation.

Figs. 4 to 6 show the effects of magnetic hysteresis and saturation on the reflected and penetrated waveforms for a very thick material. That is, in order to visualize the pulse penetration into the material, we assume $a$ is very large such that at the observation time, $t$, the pulse has not reached the metal: $a \gg 1$ and $a \gg t$. In these figures the profiles are shown at $t = 3$ and the horizontal axis is the $z$-axis. The following parameters have been used: $\chi_\epsilon = 5, x_m^{(-)} = 7$, and $\tau_e = 0.2 = \tau_m$. Fig. 3 assumes the nonsaturable case ($M_s \gg 1$) with $\chi_m^{(-)}$ varies from 7 to 3 for curves (1) to (5). It is seen that reflection tails are quite sensitive to the $\chi_m^{(-)}$ values. As $\chi_m^{(-)}$ becomes more hysteretic, the reflection tail goes more negative with the step-reflection almost unaffected. Similar results can also be found in [2]. Note that for curves (1) and (2) the characteristic impedance of the material is larger than that of air for the trailing edge reflection, while the impedance of the material is smaller than that of air for curves (4) and (5). For curve (3) the impedance is matched for trailing edge reflection, which is identified in Fig. 3 as flat transition of

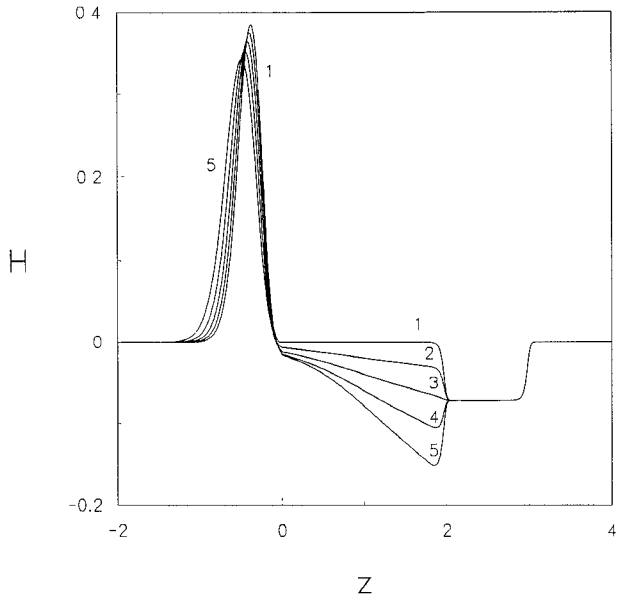


Fig. 4. Reflected and transmitted waves for nonhysteretic, curve (1), and hysteretic materials, curves (2) to (5). $\chi_e = 5$. $\chi_m^{(+)} = 7$. $\tau_e = 0.2$. $\tau_m = 0\ 2$. $M_s \gg 1$. Curve (1): $\chi_m^{(-)} = 7$. Curve (2): $\chi_m^{(-)} = 6$. Curve (3): $\chi_m^{(-)} = 5$. Curve (4): $\chi_m^{(-)} = 4$. Curve (5): $\chi_m^{(-)} = 3$.

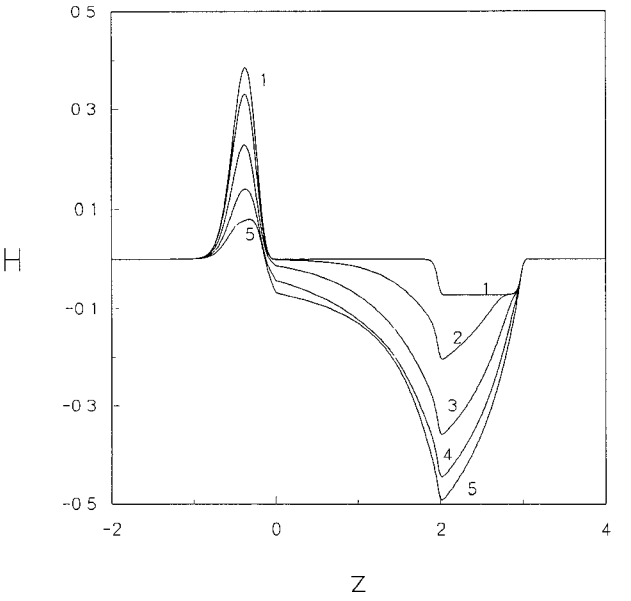


Fig. 5. Reflected and transmitted waves for saturable material: $\chi_e = 5$. $\chi_m^{(+)} = 7$. $\chi_m^{(-)} = 7$. $\tau_e = 0.2$. $\tau_m = 0\ 2$. Curve (1): $M_s = 8$. Curve (2): $M_s = 4$. Curve (3): $M_s = 2$ Curve (4): $M_s = 1$. Curve (5): $M_s = 0.5$.

the step-reflection without sudden change in tails. Therefore, by examining the shape of the reflection tails one may tell the amount of hysteresis that the trailing edge experienced upon reflection. In Fig. 4 it is seen that the penetrated wave shows decreasing amplitudes as the hysteretic effect is increased from curves (1) to (5). This is accompanied with increasing group velocities of the transmitted waves as one may expect ($\chi_m$ is effectively decreasing from curves (1) to (5)).

Fig. 5 shows the nonhysteretic case ($\chi_m^{(-)} = 7$) with $M_s$ varying from 8 to 0.5 for curves (1) to (5). It is seen that as the incident pulse amplitude goes beyond saturation, the reflected wave becomes more and more distorted and the step reflection is no more flat: the more intense the incident pulse, the more tilted the reflected step shape. Therefore, by judging from the slope of the step reflection one may tell the amount of saturation that the pulse is experienced upon reflection. The penetrated wave exhibits smaller and smaller amplitude as the input pulse amplitude goes further beyond saturation from curves (1) to (5). Fig. 6 shows the hysteretic case with saturation ($M_s = 2$). In Fig. 6 $\chi_m^{(-)}$ varies from 7 to 3 for curves (1) to (5). Both hysteretic and saturation effects can be seen in Fig. 6. Firstly, the step reflections are tilted due to magnetization saturation. Secondly, the reflection in the trailing edge becomes invisible for curve (3) where the material impedance happens to match that of air. Also, it is seen that the penetrated wave shows less transmission amplitudes as hysteresis increases, which results in increase of the group velocity for the penetrated waves. We note here that precursors associated with the penetrated signals do appear in Figs. 4 to 6. However, their magnitudes are about 1000 times weaker than the main signals, and hence they are almost invisible in these figures. Precursors signify the propagation of disturbances appearing only in frequency-dispersive materials [4].

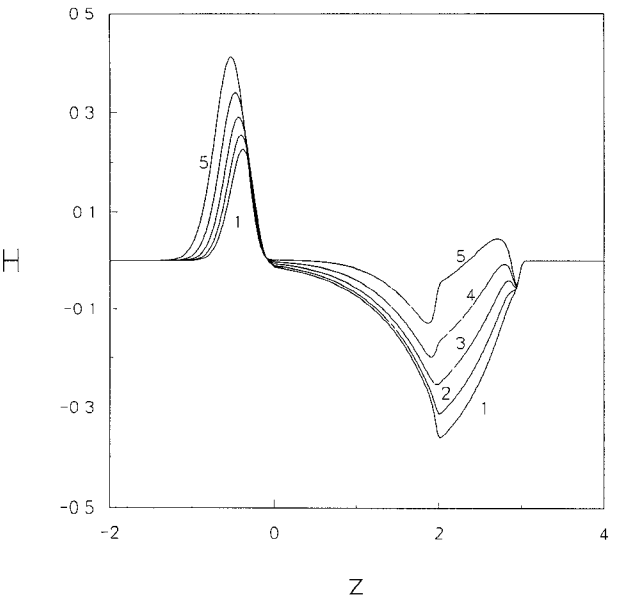


Fig. 6. Reflected and transmitted waves for hysteretic and saturable material: $\chi_e = 5$. $\chi_m^{(+)} = 7$. $\tau_e = 0.2$. $\tau_m = 0.2$. $M_s = 2$. Curve (1). $\chi_m^{(-)} = 7$. Curve (2): $\chi_m^{(-)} = 6$ Curve (3): $\chi_m^{(-)} = 5$. Curve (4): $\chi_m^{(-)} = 4$ Curve (5): $\chi_m^{(-)} = 3$.

One possible application of magnetic hysteretic materials is for screening the incident microwave pulses. For example, if we set $\chi_e$ equal to $\chi_m^{(+)}$ (such that the material impedance equals that of air) the pulse penetrates into the material without reflection. At later time (in the order of pulse width) the materials susceptibility is $\chi_m^{(-)}$ which is much different from $\chi_m^{(+)}$. This implies a characteristic impedance much different from air. Hence, the pulse is trapped. The trapped pulse is reflected back and forth within the magnetic film until it is anihilated by losses in the medium. This trapping mechanism is shown in Fig. 7 which used the following parameters:

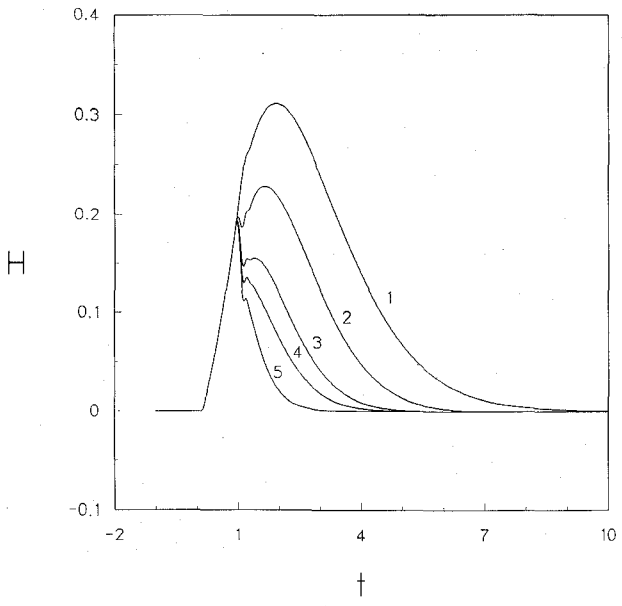


Fig. 7. Picosecond pulse screening: $\chi_e = 10, \chi_m^{(+)} = 10, \tau_e = 0.5$, $\tau_m = 0.5, a = 0.1, M_s \gg 1$. Curve (1): $\chi_m^{(-)} = 7$, Curve (1): $\chi_m^{(-)} = 10$. Curve (2): $\chi_m^{(-)} = 5$. Curve (3): $\chi_m^{(-)} = 2$. Curve (4): $\chi_m^{(-)} = 1$. Curve (5): $\chi_m^{(-)} = 0$.

$\chi_e = 10, \chi_m^{(+)} = 10, \tau_e = \tau_m = 0.5, a = 0.1$, and $M_s \gg 1$ (magnetic nonsaturable). Fig. 7 shows the reflected $H$- field as a function of time. Curves (1) to (5) are associated with decreasing $\chi_m^{(-)}$ from 10 to 0. It is seen from Fig. 7 that the screening effect of the film becomes more obvious if the material exhibits more hysteresis. When comparing curves (5) with (1) one concludes that the material absorbs 85% more energy from the incident pulse if $\chi_m^{(-)}$ is changed from 10 to 0. Magnetic hysteretic materials may lend themselves to important applications in the design of microwave absorbing materials.

## IV. Conclusion

Picosecond pulse reflection on metal-backed magneto-dielectric slabs has been calculated using direct time-domain integration. Relaxation effects as well as hysteretic and saturation effects are incorporated in the calculations. Time-domain calculations can identify the type of nonlinearities of the materials which are impinged upon by picosecond pulses. Magnetic hysteresis can significantly affect the shape of the trailing edge of the reflected signal, whereas saturation effects induce slope change in the step reflection. In addition time-domain calculations also aid in the design of microwave screening materials.

## References

[1] E. G. D. Cohen, Ed., *Fundamental Problems in Statistical Mechanics*. Amsterdam: North-Holland, 1962.
[2] H. How, F. Zayek, C. Vittoria, K. Trott, and M. Hinders, "Electromagnetic Nonlinear Responses to Picosecond Pulses," *IEEE Trans. Magn.*, vol. 27, no. 5, p. 4317, 1991.
[3] W. F. Ames, *Numerical Methods for Partial Differential Equations*, 2nd ed., New York: Academic Press, 1977, ch. 4.
[4] J. A. Stratton, *Electromagnetic Theory*. New York: McGraw-Hill, 1941, pp. 330–340.

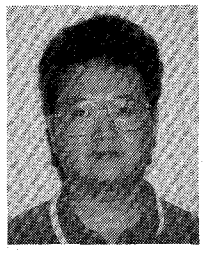

**Hoton How** received the B.S. degree in Physics from National Tsing Hua University, Taiwan, in 1976, and the Sc.D. degree in Materials Sciences and Engineering from Massachusetts Institute of Technology, MA, in 1987. Currently he is working as the senior scientist/Lecturer in the Microwave Materials Group in the Electrical and Computer Engineering Department at Northeastern University. His research interests include nonlinear ferrimagnetic phenomena, artificial materials, antennas, superconductivities, EMP effects, and various microwave/superconducting device work. Dr. How has published more than fifty refereed papers and has two US patents.

**C. Vittoria** (S'62–M'63–SM'83–F'90), photograph and biography not available at the time of publication.

**K. Trott**, photograph and biography not available at the time of publication.